# Selective entrainment of gamma subbands by different slow network oscillations

Weiwei Zhong[a,b], Mareva Ciatipis[a,c], Thérèse Wolfenstetter[a,d], Jakob Jessberger[a], Carola Müller[a], Simon Ponsel[a], Yevgenij Yanovsky[a], Jurij Brankačk[a,1,2], Adriano B. L. Tort[e,1], and Andreas Draguhn[a,1]

[a]Institute for Physiology and Pathophysiology, University of Heidelberg, 69120 Heidelberg, Germany; [b]Department of Anesthesiology, The First Affiliated Hospital of Anhui Medical University, 230022 Hefei, China; [c]Department of Neurology, Heidelberg University Hospital, 69120 Heidelberg, Germany; [d]Department of Molecular Sensory Systems, Research Center Caesar, 53175 Bonn, Germany; and [e]Brain Institute, Federal University of Rio Grande do Norte, RN 59056-450 Natal, Brazil

Edited by Nancy Kopell, Boston University, Boston, MA, and approved March 16, 2017 (received for review October 18, 2016)

**Theta oscillations (4–12 Hz) are thought to provide a common temporal reference for the exchange of information among distant brain networks. On the other hand, faster gamma-frequency oscillations (30–160 Hz) nested within theta cycles are believed to underlie local information processing. Whether oscillatory coupling between global and local oscillations, as showcased by theta-gamma coupling, is a general coding mechanism remains unknown. Here, we investigated two different patterns of oscillatory network activity, theta and respiration-induced network rhythms, in four brain regions of freely moving mice: olfactory bulb (OB), prelimbic cortex (PLC), parietal cortex (PAC), and dorsal hippocampus [cornu ammonis 1 (CA1)]. We report differential state- and region-specific coupling between the slow large-scale rhythms and superimposed fast oscillations. During awake immobility, all four regions displayed a respiration-entrained rhythm (RR) with decreasing power from OB to CA1, which coupled exclusively to the 80- to 120-Hz gamma subband ($\gamma_2$). During exploration, when theta activity was prevailing, OB and PLC still showed exclusive coupling of RR with $\gamma_2$ and no theta-gamma coupling, whereas PAC and CA1 switched to selective coupling of theta with 40- to 80-Hz ($\gamma_1$) and 120- to 160-Hz ($\gamma_3$) gamma subbands. Our data illustrate a strong, specific interaction between neuronal activity patterns and respiration. Moreover, our results suggest that the coupling between slow and fast oscillations is a general brain mechanism not limited to the theta rhythm.**

cross-frequency coupling | gamma subbands | theta | respiration | neocortex

In the rodent brain, theta oscillations (4–12 Hz) are the hallmark of the activity of neuronal networks during active behaviors and rapid eye movement (REM) sleep (1). Theta can be detected in several brain regions, and is thus thought to constitute a common temporal reference for the exchange of information among distant networks (2). Frequently, faster oscillations in the gamma-frequency range (30–160 Hz) coexist with theta and have their amplitude modulated within theta cycles (3, 4). Differently from theta, however, gamma rhythms are believed to represent local information processing (5). This assumption has led to the proposal that cross-frequency coupling between theta and gamma may integrate spatially distributed local network activity, thereby forming coherent representations within spatially extended functional networks (6). Whether the interaction between low- and high-frequency oscillations, as showcased by theta-gamma coupling, is a general coding mechanism used by the brain remains to be determined.

Rodents rely on olfaction as a major source of information for behavioral decisions (7). In mice and rats, rhythmic nasal respiration generates network oscillations at the same frequency as breathing cycles. Although such patterned network activity has long been known in primary olfactory areas such as the olfactory bulb (OB) (8) and piriform cortex (9, 10), respiration-coupled network oscillations have also recently been described in downstream regions. Specifically, a rhythmic local field potential (LFP) phase-locked to nasal respiration was found to exist and modulate spiking activity in the primary somatosensory cortex (11) and in the hippocampus (12–14), an integrative, multimodal region. Along with previous theoretical accounts (15), these studies suggest that not only theta but also the respiratory cycle may aid long-range network communication in the rodent brain.

Interestingly, theta and respiration-coupled oscillations may coexist within the same brain region (12–14). Given their distinct nature, however, each of the two low-frequency rhythms is likely to integrate different types of information. In this case, there should exist a mechanism allowing the separation of theta- and respiration-coupled rhythms and the related cognitive–behavioral functions. Based on the role of cross-frequency interactions in integrating distributed network activity (16), we hypothesized that differential coupling patterns to higher frequency oscillations may provide such a mechanism. To test this hypothesis, we performed multisite LFP recordings while concomitantly tracking respiration in freely behaving mice. Our results show that theta oscillations and the respiration-entrained rhythm (RR) modulate distinct subbands of gamma oscillations, with different spatial distribution and behavioral correlates.

## Results

We sought to map global patterns of network activity and their regional coupling to gamma oscillations. To that end, we simultaneously recorded respiration and LFPs in four brain regions of mice: OB, prelimbic cortex (PLC), parietal cortex (PAC), and cornu ammonis 1 (CA1) in the dorsal hippocampus. We examined a total of 22 freely moving mice, but different animals had electrodes in different regions; for each analysis below (i.e., behavioral state and

### Significance

Theta-gamma coupling has been largely documented in hippocampal and neocortical areas and hypothesized to constitute a network mechanism for information processing. However, we identify here another global slow rhythm at near-theta frequency that also couples to gamma. By simultaneously recording respiration, we could distinguish actual theta oscillations from a respiration-entrained rhythm (RR) in the local field potential whose peak frequency may overlap with theta. We demonstrate a robust specificity for the coupling of different gamma subbands to either theta or RR depending on brain state and region. The results suggest that the brain uses different frequency channels for transferring different types of information.

Author contributions: J.B., A.B.L.T., and A.D. designed research; W.Z., M.C., T.W., J.J., C.M., S.P., and Y.Y. performed research; J.B. and A.B.L.T. analyzed data; and J.B., A.B.L.T., and A.D. wrote the paper.

The authors declare no conflict of interest.

This article is a PNAS Direct Submission.

[1]J.B., A.B.L.T., and A.D. contributed equally to this work.

[2]To whom correspondence should be addressed. Email: jurij.brankack@physiologie.uni-heidelberg.de.

This article contains supporting information online at www.pnas.org/lookup/suppl/doi:10.1073/pnas.1617249114/-/DCSupplemental.

recorded region), the exact number is stated, along with the corresponding result. Depending on the behavioral state, LFPs in all recorded regions exhibit theta (4–12 Hz) as well as RR (>1 Hz, discussed below). Both patterns may partially or completely overlap in frequency and can only be disentangled by simultaneous recording of nasal respiration and hippocampal LFPs, as shown earlier in mice (12, 13, 17) and rats (14). RR and theta are most pronounced in different behavioral states: RR dominates brain activity during awake immobility, whereas theta is prominent during exploration (13). Therefore, we focus our analysis on these two exemplary states to investigate the interaction of different global slow rhythms with three distinct subbands of gamma oscillations: $\gamma_1$ (40–80 Hz), $\gamma_2$ (80–120 Hz), and $\gamma_3$ (120–160 Hz). In Figs. S1–S9, we show complementary results from other behavioral states.

**RR Specifically Couples to $\gamma_2$ (80–120 Hz).** In awake immobile mice, RR dominated LFPs in all recorded regions (OB, PLC, PAC, and CA1), whereas theta was mostly absent [raw data in Fig. 1*A* and power spectral densities (PSDs) in Fig. 1*B*]. Wavelet spectrograms revealed gamma activity in two distinguishable subbands, one between 40 and 80 Hz ($\gamma_1$) and another between 80 and 120 Hz ($\gamma_2$). In OB and PLC, the $\gamma_2$ amplitude was visibly phase-locked to the phase of the respiratory cycles (Fig. 1*A*). Cross-frequency comodulograms confirmed phase-amplitude coupling between RR and $\gamma_2$ (3) (*Methods* and Fig. 1*B*). Interestingly, the analysis revealed the same coupling pattern in PAC and CA1, albeit more than fivefold weaker than in OB and PLC (scaling in Fig. 1*B*). During non-REM (NREM) sleep, RR-$\gamma_2$ coupling persisted in OB and PLC and decreased in PAC and CA1 (Fig. S1).

**Theta Rhythm Couples to $\gamma_1$ (40–80 Hz) and $\gamma_3$ (120–160 Hz).** We next analyzed periods in which mice exhibited explorative activity, characterized by locomotion and simultaneous odor sampling through sniffing. During this state of sensorimotor activity, in contrast to awake immobility, respiration frequency often exceeded theta frequency (Fig. 2 and Fig. S2). Similar to immobility, $\gamma_2$ was prominent in both OB and PLC during exploration and synchronized to respiration (Fig. 2*A*). In this behavioral state, however, PSDs of LFPs in OB and PLC revealed two peaks, indicating the simultaneous presence of independent theta and RR (13) (Fig. 2*B*, solid line). Consistent with previous reports (12–14), theta and RR power levels were not correlated during exploration ($n = 8$; for each animal, power was computed in 30 nonoverlapping 1-s windows; mean $r^2 = 0.034 \pm 0.017$, range: 0.002–0.136). In OB, cross-frequency comodulograms revealed exclusive coupling between RR and $\gamma_2$ (Fig. 2*B*). Interestingly, despite the fact that during exploration theta power was higher than RR power in PLC ($n = 7$; $P < 0.0005$, paired $t$ test; Figs. 2*B* and 3*A*), $\gamma_2$ also coupled exclusively to RR but not to theta (Fig. 2*B*), indicating that the preferred coupling pattern is not primarily a function of the dominant low-frequency power. In contrast, in PAC and CA1, where RR power was much lower than theta power (PAC: $n = 7$, $P < 0.005$; CA1: $n = 10$, $P < 0.0005$, paired $t$ tests; Fig. 3*A*), $\gamma_1$ coupled exclusively to theta but not to RR (Fig. 2*B*). RR-$\gamma_2$ coupling and theta-$\gamma_1$/$\gamma_3$ coupling were not dependent on running speed (but see ref. 18) (Fig. S3). In PAC, the theta phase also weakly modulated the $\gamma_3$ (120–160 Hz) amplitude during exploration; such modulation substantially increased during REM sleep (19) (Fig. S4). We found similar results when animals were sniffing during periods of low locomotion; namely, RR modulated $\gamma_2$ mostly in OB and PLC, whereas theta modulated $\gamma_1$ and $\gamma_3$ mostly in CA1 and PAC (Fig. S5). Variations of theta and RR power and coupling strength across behavioral states are shown in Figs. S6 and S7, respectively.

**Exclusive Coupling of Specific Gamma Subbands to Theta and Respiration.** To quantify the coupling preference of the three subbands of gamma to either theta or RR, we calculated a modulation ratio for each region; for each gamma subband, the modulation ratio normalizes its coupling strength by the sum of all gamma subbands (*Methods*). Preferential coupling of gamma to theta results in positive modulation ratios, whereas stronger coupling to RR leads to negative ratios. Fig. 3 *B* and *C* shows group data for coupling between slow and fast oscillations during awake immobility and exploration. Preferential coupling of $\gamma_2$ to RR was significant in all four regions during awake immobility (Fig. 3*C*, *Left*; OB: $n = 8$, $P < 0.0005$; PLC: $n = 9$, $P < 0.0005$; PAC: $n = 7$, $P < 0.0005$; CA1: $n = 9$, $P < 0.005$; one-way ANOVA with Dunnett's multiple comparisons test). Similar results were found during NREM sleep (Fig. S8).

During exploration, the preferred pattern of cross-frequency coupling had a different signature. In this state, coupling of $\gamma_2$ with RR was restricted to OB and PLC (Fig. 3*C*, *Right*; OB, PLC: $n = 7$, $P < 0.0005$; one-way ANOVA with Dunnett's multiple comparisons test). In contrast, PAC and CA1 displayed preferred coupling of $\gamma_1$ with theta (Fig. 3*C*, *Right*; PAC: $n = 7$, $P < 0.0005$; CA1: $n = 10$, $P < 0.0005$; one-way ANOVA with Dunnett's multiple comparisons test). Similar results were found in all regions during sniffing with minimal locomotion (Fig. S9).

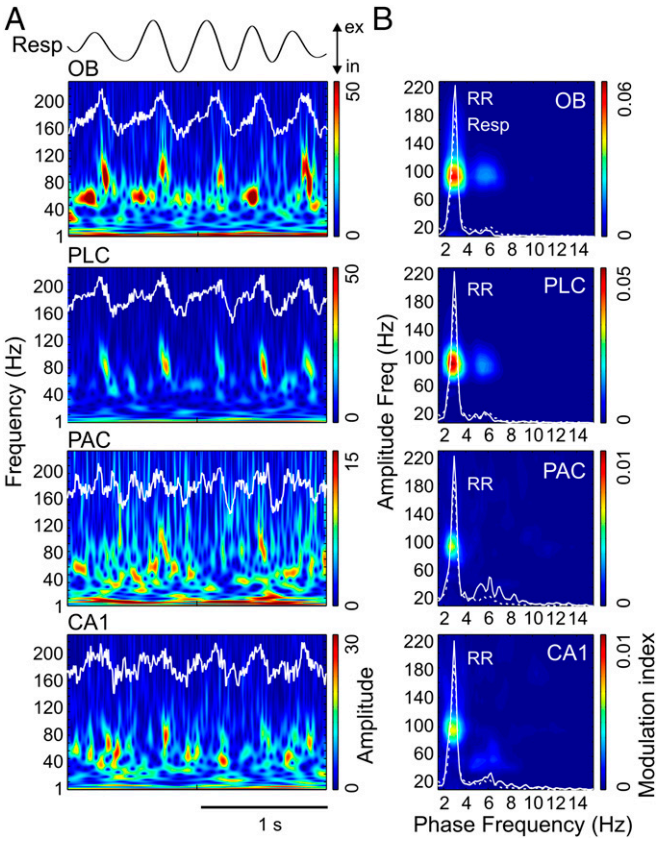


**Fig. 1.** Specific coupling between RR and $\gamma_2$ (80–120 Hz) during immobility. (*A*) Wavelet spectrograms and superimposed LFP signals (white traces) from OB, PLC, PAC, and CA1 simultaneously recorded during awake immobility. The top trace shows nasal respiration (Resp) signal. ex, exhalation; in, inhalation. Note the presence of two subbands of gamma oscillations in OB: 40–80 Hz ($\gamma_1$) and 80–120 Hz ($\gamma_2$). (*B*) Pseudocolor maps depict cross-frequency comodulograms computed during immobility; warm colors denote phase-amplitude coupling (*Methods*). For each region, the superimposed white lines depict PSDs of LFPs (continuous line) and Resp (dashed line; same for all regions) plotted in different *y*-axis scales to allow inspection of power peaks. The peak of the dashed line indicates breathing rate (~3 Hz in this example); all LFPs exhibit a power peak at the same frequency, which corresponds to RR. Notice specific coupling of $\gamma_2$ to RR in the comodulograms and that coupling strength decreases from OB/PLC to PAC/CA1. All plots were obtained from the same epoch (group data are shown in Fig. 3).

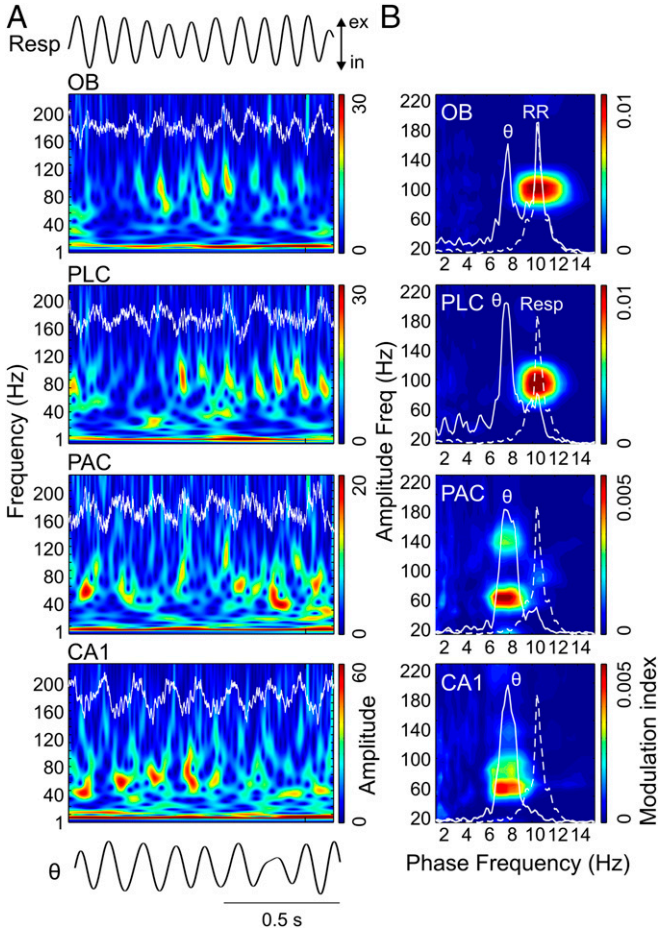


**Fig. 2.** Region-specific and slow oscillation-specific coupling of different gamma subbands during exploration. (*A*) Wavelet spectrograms and OB, PLC, PAC, and CA1 LFPs (white traces) simultaneously recorded during spatial exploration. The top and bottom traces depict Resp and the theta-filtered LFP (θ) signal, respectively. ex, exhalation; in, inhalation; Resp, respiration. (*B*) Cross-frequency comodulograms, along with power spectra of LFPs (continuous white line) and Resp (dashed white line; same for all regions), computed during exploration. In this example, respiration frequency (i.e., peak of the dashed-line spectrum) is faster (~10 Hz) than theta oscillations (~8 Hz, peak of the continuous-line spectrum in CA1). The OB LFP exhibits a power peak at theta and another at the respiration frequency, which corresponds to RR. PLC and PAC LFPs also exhibit power peaks at theta and RR, but the latter has much lower magnitude. In CA1, only a power peak at theta can be observed. The comodulograms show that $\gamma_2$ (80–120 Hz) couples specifically to RR in OB and PLC, whereas $\gamma_1$ (40–80 Hz) and $\gamma_3$ (120–160 Hz) couple specifically to theta in PAC and CA1. All plots were obtained from the same epoch (group data are shown in Fig. 3).

During REM sleep, theta recorded in PAC and CA1 was also preferentially coupled to $\gamma_1$ (Fig. S8; PAC: $n = 8$, $P < 0.005$; CA1: $n = 7$, $P < 0.0005$; one-way ANOVA with Dunnett's multiple comparisons test). In addition, PAC displayed significant preferred coupling between theta and $\gamma_3$ (Fig. S8; PAC: $n = 8$, $P < 0.0005$; one-way ANOVA with Dunnett's multiple comparisons test). On the other hand, during REM sleep, the coupling preference for RR-$\gamma_2$ in OB and PLC was significantly diminished compared with NREM sleep (Fig. S8; OB: $n = 6$ and 7, $P < 0.0005$; PLC: $n = 6$ and 8, $P < 0.0005$; unpaired $t$ tests). Table 1 presents a summary of the preferred coupling patterns in each region and behavioral state.

**Neocortical Units Couple to Respiration and Theta.** We have previously shown that respiration modulates spiking probability in the hippocampus, and that RR in this region is not volume-conducted but locally generated (12–14). This finding suggests that RR can dominate local network activity and also entrain neurons in the neocortical regions. To investigate this possibility, we next recorded action potentials in PAC, PLC, and infralimbic cortex (ILC) from 16 urethane-anesthetized mice. A total of 22 neurons in PLC/ILC (eight in PLC and 14 in ILC) and 33 neurons in PAC were intracellularly or juxtacellularly recorded in the presence of both RR and theta, and 11 additional PLC/ILC units (five in PLC and six in ILC) were recorded in the absence of theta. Fig. 4 shows examples of units coupled to respiration in PAC (Fig. 4*A*) and ILC (Fig. 4*B*). Action potentials of seven (32%) PLC/ILC neurons significantly ($P < 0.05$, Rayleigh test) coupled to respiration alone, five (23%) coupled to theta alone, and four (18%) coupled to both rhythms (Fig. 4*C*, *Right*). Five (45%) PLC/ILC neurons recorded in the absence of theta were significantly coupled to respiration. In PAC, five (15%) neurons were significantly coupled to respiration alone, two (6%) were coupled to theta alone, and one (3%) was coupled to both rhythms (Fig. 4*C*, *Left*). Interestingly, one intracellular recording of a PAC neuron revealed membrane potential oscillations synchronous with respiration and local RR (Fig. S10). Consistent with local generation of rhythmic activity in PAC, RR could also be detected with bipolar recordings (Fig. S11).

Finally, we recorded juxtacellularly from 30 PLC neurons in four awake animals under head-fixed conditions with both RR and theta rhythms present (13). Five neurons (17%) showed significant

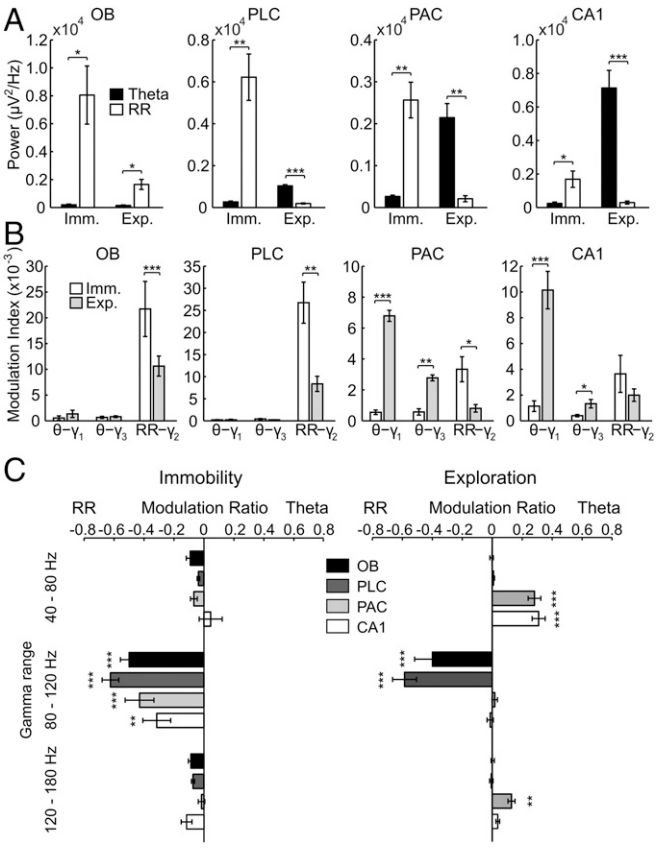


**Fig. 3.** Regional and state specificity of modulation of gamma subbands by either theta or respiration. Theta and RR power (*A*) and strength of theta-$\gamma_1$, theta-$\gamma_3$, and RR-$\gamma_2$ coupling (*B*) during immobility (Imm.) and exploration (Exp.) are shown (mean over animals: $*P < 0.05$, $**P < 0.005$, and $***P < 0.0005$; Wilcoxon signed rank or paired $t$ test in *A* and Mann–Whitney or unpaired $t$ test in *B*; $n = 7$–10). (*C*) Mean modulation ratios (*Methods* and main text). Positive ratios reflect modulation by theta, and negative ratios reflect modulation by RR. Asterisks show significant differences from zero ($**P < 0.005$ and $***P < 0.0005$; one-way ANOVA and Dunnett's multiple comparisons test; $n = 7$–10). In *A*–*C*, error bars represent SEM.

**Table 1. Preferred coupling pattern per behavioral state and brain region**

| Region | Immobility | Exploration | Sniffing | REM sleep | NREM sleep |
|---|---|---|---|---|---|
| OB | RR-$\gamma_2$ | RR-$\gamma_2$ | RR-$\gamma_2$ | — | RR-$\gamma_2$ |
| PLC | RR-$\gamma_2$ | RR-$\gamma_2$ | RR-$\gamma_2$ | — | RR-$\gamma_2$ |
| PAC | RR-$\gamma_2$ | θ-$\gamma_1$, θ-$\gamma_3$ | θ-$\gamma_1$ | θ-$\gamma_1$, θ-$\gamma_3$ | — |
| CA1 | RR-$\gamma_2$ | θ-$\gamma_1$ | θ-$\gamma_1$ | θ-$\gamma_1$ | — |

coupling to respiration alone, eight (27%) showed significant coupling to theta alone, and seven (23%) showed significant coupling to both rhythms (Fig. S12).

## Discussion

Local, higher frequency network activity usually couples to the phase of slower brain rhythms (20). Such cross-frequency coupling has previously been hypothesized to underlie information transfer between brain regions (16). For instance, theta-gamma coupling has been related to cognitive functions, including working memory (21–24). Our findings now reveal that nonoverlapping gamma channels may be used by different low-frequency rhythms, theta and RR, shedding light on the functional role of gamma oscillations and phase-amplitude coupling. In brief, we found that distinct subbands of gamma couple to either theta or RR in a state- and region-specific manner. In the absence of theta, all recorded regions exhibit RR activity, which exclusively modulates 80- to 120-Hz ($\gamma_2$) oscillations. In the presence of both theta and RR, frontal and limbic regions split into two patterns of preferential coupling: The former (OB and PLC) shows exclusive coupling of RR with $\gamma_2$ oscillations and no theta-gamma coupling, whereas the latter (PAC and CA1) exhibits exclusive coupling of theta with 40- to 80- Hz ($\gamma_1$) and 120- to 160-Hz ($\gamma_3$) oscillations (Table 1).

We have recently reported RR as a hippocampal oscillation pattern in anesthetized (12) and awake head-fixed mice (13). We showed that RR and theta could simultaneously exist within the same temporal epoch but that they nevertheless differed from each other in various ways: Despite having similar frequency ranges, both patterns show clearly distinct current-source density and voltage-depth profiles, resistance to atropine, coherence to respiration, and dependence on nasal airflow (12–14). Here, we expand our previous results by showing that each rhythm modulates specific gamma subbands in freely moving mice, and that RR also occurs and modulates spiking probability in the medial prefrontal and parietal cortices.

Of note, Ito et al. (11) reported RR in the whisker barrel cortex of awake head-fixed mice, and Heck et al. (25) recently described significant coupling of respiration with field potentials and unit discharges also in prefrontal, somatosensory, and primary visual cortices. In addition, intracranial recordings from the piriform cortex, amygdala, and hippocampus of patients with medically refractory epilepsy revealed LFP activity synchronized with nasal, but not oral, inhalation (26). Consistent with these findings, we show here that respiration-entrained oscillations are detectable in nonrestrained animals and extend to cortical regions downstream of primary olfactory areas, such as PLC and PAC, where they modulate neuronal activity. Together, the results suggest that not only theta but also RR constitutes a global brain signal and, as such, are likely to play a role in coordinating network communication across distant regions. Most importantly, theta and RR modulate gamma activity in a region- and state-specific manner, indicative of selective local computations in the respective networks (16).

We have used a neutral definition for the gamma subbands ($\gamma_{1-3}$) to avoid confusion with previous notations (4, 18, 22, 27, 28). In any case, there was a clear separation of coupling patterns between distinct gamma subbands and the slow oscillations. We hypothesize that coupling between different frequency channels allows the simultaneous integration of different types of information across distant networks without interference. Accordingly, it has previously been argued that different gamma subbands reflect specific operational modes or inputs (5). Moreover, different gamma frequencies have been shown to take part in the communication within the hippocampal formation (29). Our results extend these observations by showing that there are distinct subbands not only for the amplitude-modulated, fast-carrier frequencies (i.e., different gammas) but also for the phase-modulating, slow frequencies (i.e., theta vs. RR), which should work as complementary mechanisms for the multiplexing of information.

It should be noted that breathing rate and RR often exhibit an overlapping frequency range with theta oscillations. Because RR also modulates gamma activity, it is possible that previous reports on theta-gamma coupling may have actually described RR-gamma coupling (in the present work, we only analyzed periods in which respiration and theta frequencies were nonoverlapping; *Methods*). For instance, we described a "slow theta" oscillation (4–6 Hz) in striatum that modulated 80- to 120-Hz oscillations (22); moreover, the peak frequency of the slow theta activity increased as animals ran on a T-maze (figure 1 of ref. 22). In hindsight, we now suspect

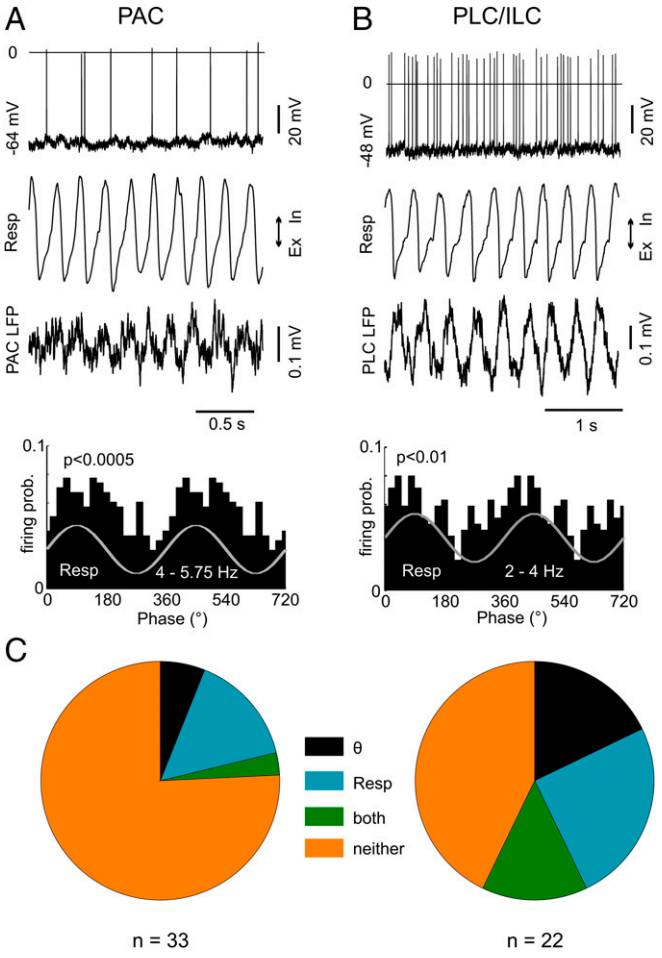


**Fig. 4.** RR and theta rhythms modulate spiking of neurons in PAC and PLC/ILC. (*A*, *Top*) Intracellular recording from a neuron in PAC significantly modulated by respiration (Resp). (*A*, *Middle*) Resp and PAC LFP signals. (*A*, *Bottom*) Spike distribution over the phases of respiration cycles. (*B*) As in *A*, but for a neuron in the ILC. Ex, exhalation; In, inhalation; prob., probability. (*C*) Percentage of significantly modulated units in PAC (*Left*) and PLC/ILC (*Right*) by theta (θ) alone, by Resp alone, by both rhythms, or by neither rhythm.

that the slow theta corresponds to RR, that the observed comodulation corresponds to RR-$\gamma_2$ coupling, and that the change in slow theta frequency reflects changes in breathing rate. Similarly, Zhang et al. (30) reported that lack of amyloid precursor protein (APP) leads to impaired theta-gamma coupling in CA1 and PAC, but not in PLC. It is possible that the theta-gamma coupling in PLC reported in this study actually corresponds to RR-$\gamma_2$ coupling. Without concomitant measurements of respiration, however, it is difficult to distinguish RR from theta.

The coexistence of RR and theta in the PLC should also be taken into account when interpreting previous results on cross-regional synchronization of LFP oscillations. For instance, oscillations in the theta frequency range have been shown to synchronize the medial prefrontal cortex, ventral hippocampus, and amygdala during working memory (31) and fear/anxiety-related behavior (32). In addition, 4-Hz oscillations have been described to link network activity in the ventral tegmental area, prefrontal cortex, and hippocampus of rats (33), and would coordinate prefrontal-amygdala circuits during fear behavior in mice (34, 35). We suspect that the slow oscillations reported in these studies correspond to RR, that is, LFP activity coupled to respiration. Unfortunately, because respiration was not simultaneously recorded, this possibility remains to be tested.

In summary, we have shown that theta and respiration-coupled rhythms are two separate long-range signals that differentially modulate network activity in distinct gamma channels. The specific patterns of cross-frequency coupling depend on the recorded region and behavioral state. These results support the hypothesis that network communication relies on neuronal oscillations at multiple scales, which are likely involved in the integration of local and distributed processing.

## Methods

In short, we recorded LFPs from OB, PLC, PAC, and hippocampus of 22 moving mice in various behavioral and vigilance states. In all animals, thermocouples (TCs) were chronically implanted into the nasal cavity to measure respiratory activity simultaneously with LFPs. For unit recordings, an additional 16 mice were anesthetized with urethane (12) and an additional four awake animals were used in head-fixed conditions (13). Below and in *SI Methods*, we provide further methodological details.

**Ethics Statement.** This study was carried out in accordance with the guidelines of the European Science Foundation (36) and the US NIH *Guide for the Care and Use of Laboratory Animals* (37), and it has been approved by the Governmental Supervisory Panel on Animal Experiments of Baden Württemberg at Karlsruhe (35-9185.81/G-84/13). All efforts were made to minimize animal suffering and to reduce the number of animals used. Due to the systemic approach of the study, alternatives to in vivo techniques were not available.

**Animal Care and Housing Conditions.** C57BL/6N mice were purchased at 70 or 84 d of age from Charles River Laboratories. Animals were housed in groups of four inside a ventilated Scantainer (Scanbur BK A/S Denmark) on an inverted 12/12-h light/dark cycle (light on at 8:00 PM) for a minimum of 2 wk. Animals had free access to water and food. After chronic electrode implantation, mice were housed individually throughout the experiment. The animals were killed with an overdose of isoflurane during brain perfusion.

**Animal Preparation.** We used 22 C57BL/6N (19 female and three male) mice in freely moving experiments and 20 C57BL/6N (16 female and four male) mice for recordings under urethane anesthesia or head-fixed conditions. Animals weighed 20–30 g and were 12–20 wk of age. The animals used in freely moving experiments were anesthetized with isoflurane in medical oxygen (4% isoflurane for induction, 1.5–2.5% for maintenance, flow rate of 1 L·min$^{-1}$). For analgesia, 0.1 mg/kg of buprenorphine was injected s.c. before and 8 h after surgery. Anesthetized animals were mounted on a stereotaxic apparatus (Kopf Instruments) with a custom-made inhalation tube. Body temperature was maintained at 38 °C by a heating pad (ATC-2000; World Precision Instruments). After exposure of the skull, holes sized 0.5–1.0 mm in diameter were drilled above the dorsal hippocampus, OB, PLC, and PAC according to stereotaxic coordinates (38). Two stainless-steel watch screws (1 × 3 mm) over the cerebellum served as ground and reference electrodes. For monitoring the temperature of nasal airflow, two precision fine-bare wire TCs (80 μm in diameter, part no. 5TC-TT-KI-40-1M; Omega Engineering, Inc.) were implanted into the right and left nasal cavities (11 mm anterior, 0.5 mm mediolateral). Pairs of varnish-insulated tungsten wires (50 μm, glued together) cut at an angle of 45° were implanted into the right OB (4.5 mm anterior, 0.8 mm lateral, 0.8–1.3 mm ventral), right PLC (1.8 mm anterior, 0.3 mm lateral, 1.9–2.2 mm ventral), and right dorsal hippocampal CA1/dentate gyrus area (2.0 mm posterior, 1.5 mm lateral, 1.5–2.5 mm ventral). A stainless-steel watch screw was placed above the left PAC (2 mm posterior, 2 mm lateral) to record from the cortical surface. Details on preparations and recordings for head-fixed and acute experiments are provided in *SI Methods*.

**Electrophysiology in Freely Moving Mice.** Six days to 7 d after surgery, experiments began with continuous monopolar intracranial electroencephalographic recordings in the animal's home cage. Respiration was simultaneously recorded using nasal TCs. The animal's behavior was recorded by an Ethovision XT 9 (Noldus Information Technology) video-tracking system, and movements were detected by 3D accelerometry. To collect periods of exploration, sniffing, awake immobility, and NREM and REM sleep (criteria for behavioral staging are discussed below), recording sessions of up to 4 h were performed in the animal's home cage on consecutive days. Sniffing and exploration were most intense during the first recording session. For a fixed brain region and behavioral state, each animal contributed a single LFP sample, which fulfilled the following criteria: (*i*) the animal behavior had to be clearly staged; (*ii*) the TC and LFP signals had to be deemed "artifact-free" upon visual inspection; (*iii*) for periods of theta activity, respiration frequency (inferred by the power spectrum of the TC signal) and theta frequency (inferred by the power spectrum of CA1) could not be overlapping. To avoid bias due to differences in epoch length, the analyzed epoch length was fixed at 30 s for each LFP sample (3, 30). For immobility and NREM sleep, we selected the first 30-s epoch that fulfilled the criteria above; for the other periods, we selected the 30-s epoch with largest frequency difference between respiration and theta. TC signals and OB LFPs reliably reflect respiration during waking and most of REM sleep but may deteriorate during deep NREM sleep (17). Therefore, additional recordings were performed in a whole-body plethysmograph (EMKA Technologies, S.A.S.); details are provided elsewhere (17). Extracellular signals were filtered (1–500 Hz), amplified (RHA2116 Intan Technologies, LLC), digitized (2.5 kHz), and stored for offline analyses with custom-written MATLAB routines (The Mathworks, Inc.).

**Data Analysis.** The data were analyzed in MATLAB using built-in and custom-written routines.

***Behavioral staging.*** Classification of vigilance states was based on (*i*) the level of accelerometer activity (exploration, sniffing > awake immobility, NREM, REM), (*ii*) the amount of high-amplitude slow-wave activity in the neocortex (NREM > waking, REM), and (*iii*) the amount of regular theta oscillations in PAC overlaying the dorsal hippocampus (exploration, REM > sniffing > awake immobility, none in NREM). Awake immobility was defined as the absence of any prominent accelerometer signals and any slow-wave (delta) activity indicating sleep. A detailed description of behavioral staging is provided elsewhere (17, 39) and in *SI Methods*.

***Spectral analysis.*** PSD was calculated by means of the Welch periodogram method using the *pwelch.m* function from the Signal Processing Toolbox (50% overlapping, 4-s Hamming windows). In Fig. 3*A* and Fig. S6, theta and RR peak power was estimated by first subtracting the fitting of the reciprocal of frequency (1/f) over 2–30 Hz from the PSD; for each region, RR peak power was then taken as the corrected PSD value at the respiration frequency, whereas theta peak power was taken as the corrected PSD value at the same frequency as the highest CA1 power peak in the 4- to 12-Hz range. The time-frequency decompositions shown in Figs. 1 and 2 were obtained by continuous wavelet transform. To that end, LFP or respiration signals were convoluted with complex Morlet wavelets with central frequencies ranging from 1 to 220 Hz in 1-Hz steps. For a fixed frequency, the instantaneous energy was taken as the absolute value of the transform at each time point.

***Cross-frequency coupling.*** To measure the intensity of phase-amplitude coupling, we used the modulation index (MI) described in detail elsewhere (3). The MI measures coupling between two frequency ranges of interest: a slower phase-modulating ($f_p$) and a faster amplitude-modulated ($f_a$) frequency. Briefly, the MI is computed as follows: the phases of $f_p$ are binned into eighteen 20° intervals, and the mean amplitude of $f_a$ in each phase bin is determined. The mean $f_a$ amplitude in each phase bin is normalized so that its sum over all phase bins equals 1. This procedure gives rise to a phase-amplitude "distribution." A uniform phase-amplitude distribution means that the $f_a$ amplitude is, on average, the same for all $f_p$ phases, which happens in the absence of phase-amplitude coupling. The higher the coupling, the further away the phase-amplitude distribution gets from the uniform distribution. The MI measures the divergence of

the phase-amplitude distribution from the uniform distribution (3). Of note, because the MI formula relies on measuring (and normalizing) entropy, this metric is highly nonlinear and accentuates the difference between weak and strong coupling compared with measures based on assessing the peak and trough values of the phase-amplitude distribution (3). The comodulogram (Fig. 1*B*) is obtained by computing the MI of several frequency band pairs and expressing the results in a 2D pseudocolor plot. One dimension denotes the frequency bands analyzed as phase-modulating, and the other dimension represents the amplitude-modulated bands. The frequency bands are narrow-filtered (phase frequencies: 4-Hz bandwidths; amplitude frequencies: 10-Hz bandwidths), and each coordinate in the comodulogram represents the center frequency. A warm color in an ($f_p$,$f_a$) entry of the comodulogram means that the phase of $f_p$ modulates the amplitude of $f_a$.

***Modulation ratio.*** To compare the coupling strength of RR/gamma vs. theta/gamma, we computed a modulation ratio for each recorded region (OB, PLC, PAC, and CA1), behavioral state (immobility, exploration, REM, and NREM), and gamma range ($\gamma_1$, $\gamma_2$, and $\gamma_3$). For a fixed region, behavioral state, and gamma range, the modulation ratio is obtained by subtracting RR/gamma$^j$ MI from theta/gamma$^j$ MI, where *j* indexes the gamma range, normalizing by the sum of MI values over all gamma ranges:

$$Modulation\ Ratio = \frac{MI_{theta/gamma^j} - MI_{RR/gamma^j}}{\sum_j MI_{theta/gamma^j} + MI_{RR/gamma^j}}$$

The modulation ratio varies between −1 and 1. Positive values indicate that theta/gamma$^j$ coupling is stronger than RR/gamma$^j$ coupling; conversely, negative values indicate that RR/gamma$^j$ coupling is stronger.

***Spike-phase coupling.*** Spike-phase coupling was assessed as described elsewhere (13). In brief, we first band-pass-filtered the LFP within the frequency range of interest (*eegfilt* function from the EEGLAB toolbox; https://sccn.ucsd.edu/eeglab/) and then extracted the phase time series using the Hilbert transform (*hilbert.m* function). The spike-phase histogram is obtained by counting the phases associated with spike times, and its significance is determined by the Rayleigh test for circular uniformity.

***Histology.*** After the conclusion of the experiments, the animals were deeply anesthetized with isoflurane and perfused transcardially with PBS and subsequently with 4% paraformaldehyde (PFA). Brains were carefully dissected and stored in PFA overnight, and coronal sections were cut (50 μm), mounted, and stained with cresyl violet. The position of single electrodes and multichannel electrode probes was then verified by light microscopy.

***Statistics.*** Data are expressed as means and SEM. For group comparisons of normally distributed data (Kolmogorov–Smirnov test), we used a *t* test or one-way ANOVA, followed by correction tests for multiple comparisons. For data with a non-Gaussian distribution, we used the nonparametric Mann–Whitney test, the Wilcoxon signed rank test, or the Kruskal–Wallis one-way analysis of variance. Significances are shown with asterisks (*$P < 0.05$, **$P < 0.005$, ***$P < 0.0005$).

**ACKNOWLEDGMENTS.** This work was supported by the Deutsche Forschungsgemeinschaft (SFB 636/B06, SFB 1134/A01, Dr 326/10-1), Bundesministerium für Bildung und Forschung (Bernstein Center for Computational Neurosciences Grant 01GQ1003A, German-Brazil Cooperation Grant 01DN12098), Brazilian National Council for Scientific and Technological Development, Brazilian Coordination for the Improvement of Higher Education Personal, and Alexander von Humboldt Foundation. W.Z. was supported by the China Scholarship Council.

1. Buzsáki G (2002) Theta oscillations in the hippocampus. *Neuron* 33:325–340.
2. Buzsáki G (2010) Neural syntax: Cell assemblies, synapsembles, and readers. *Neuron* 68:362–385.
3. Tort ABL, Komorowski R, Eichenbaum H, Kopell N (2010) Measuring phase-amplitude coupling between neuronal oscillations of different frequencies. *J Neurophysiol* 104: 1195–1210.
4. Tort ABL, Scheffer-Teixeira R, Souza BC, Draguhn A, Brankačk J (2013) Theta-associated high-frequency oscillations (110-160Hz) in the hippocampus and neocortex. *Prog Neurobiol* 100:1–14.
5. Buzsáki G, Wang X-J (2012) Mechanisms of gamma oscillations. *Annu Rev Neurosci* 35: 203–225.
6. Igarashi J, Isomura Y, Arai K, Harukuni R, Fukai T (2013) A θ-γ oscillation code for neuronal coordination during motor behavior. *J Neurosci* 33:18515–18530.
7. Qiu Q, et al. (2014) Automated analyses of innate olfactory behaviors in rodents. *PLoS One* 9:e93468.
8. Adrian ED (1950) The electrical activity of the mammalian olfactory bulb. *Electroencephalogr Clin Neurophysiol* 2:377–388.
9. Fontanini A, Spano P, Bower JM (2003) Ketamine-xylazine-induced slow (<1.5 Hz) oscillations in the rat piriform (olfactory) cortex are functionally correlated with respiration. *J Neurosci* 23:7993–8001.
10. Fontanini A, Bower JM (2006) Slow-waves in the olfactory system: An olfactory perspective on cortical rhythms. *Trends Neurosci* 29:429–437.
11. Ito J, et al. (2014) Whisker barrel cortex delta oscillations and gamma power in the awake mouse are linked to respiration. *Nat Commun* 5:3572.
12. Yanovsky Y, Ciatipis M, Draguhn A, Tort ABL, Brankačk J (2014) Slow oscillations in the mouse hippocampus entrained by nasal respiration. *J Neurosci* 34:5949–5964.
13. Nguyen Chi V, et al. (2016) Hippocampal respiration-driven rhythm distinct from theta oscillations in awake mice. *J Neurosci* 36:162–177.
14. Lockmann ALV, Laplagne DA, Leão RN, Tort ABL (2016) A respiration-coupled rhythm in the rat hippocampus independent of theta and slow oscillations. *J Neurosci* 36:5338–5352.
15. Kepecs A, Uchida N, Mainen ZF (2006) The sniff as a unit of olfactory processing. *Chem Senses* 31:167–179.
16. Canolty RT, Knight RT (2010) The functional role of cross-frequency coupling. *Trends Cogn Sci* 14:506–515.
17. Jessberger J, Zhong W, Brankačk J, Draguhn A (2016) Olfactory bulb field potentials and respiration in sleep-wake states of mice. *Neural Plast* 2016:4570831.
18. Chen Z, Resnik E, McFarland JM, Sakmann B, Mehta MR (2011) Speed controls the amplitude and timing of the hippocampal gamma rhythm. *PLoS One* 6:e21408.
19. Scheffzük C, et al. (2011) Selective coupling between theta phase and neocortical fast gamma oscillations during REM-sleep in mice. *PLoS One* 6:e28489.
20. Lakatos P, et al. (2005) An oscillatory hierarchy controlling neuronal excitability and stimulus processing in the auditory cortex. *J Neurophysiol* 94:1904–1911.
21. Mormann F, et al. (2005) Phase/amplitude reset and theta-gamma interaction in the human medial temporal lobe during a continuous word recognition memory task. *Hippocampus* 15:890–900.
22. Tort ABL, et al. (2008) Dynamic cross-frequency couplings of local field potential oscillations in rat striatum and hippocampus during performance of a T-maze task. *Proc Natl Acad Sci USA* 105:20517–20522.
23. Tort ABL, Komorowski RW, Manns JR, Kopell NJ, Eichenbaum H (2009) Theta-gamma coupling increases during the learning of item-context associations. *Proc Natl Acad Sci USA* 106:20942–20947.
24. Colgin LL (2015) Theta-gamma coupling in the entorhinal-hippocampal system. *Curr Opin Neurobiol* 31:45–50.
25. Heck DH, et al. (2016) Cortical rhythms are modulated by respiration. *bioRxiv*, 10.1101/049007.
26. Zelano C, et al. (2016) Nasal respiration entrains human limbic oscillations and modulates cognitive function. *J Neurosci* 36:12448–12467.
27. Scheffer-Teixeira R, et al. (2012) Theta phase modulates multiple layer-specific oscillations in the CA1 region. *Cereb Cortex* 22:2404–2414.
28. Belluscio MA, Mizuseki K, Schmidt R, Kempter R, Buzsáki G (2012) Cross-frequency phase-phase coupling between θ and γ oscillations in the hippocampus. *J Neurosci* 32: 423–435.
29. Colgin LL, et al. (2009) Frequency of gamma oscillations routes flow of information in the hippocampus. *Nature* 462:353–357.
30. Zhang X, et al. (2016) Impaired theta-gamma coupling in APP-deficient mice. *Sci Rep* 6:21948.
31. O'Neill P-K, Gordon JA, Sigurdsson T (2013) Theta oscillations in the medial prefrontal cortex are modulated by spatial working memory and synchronize with the hippocampus through its ventral subregion. *J Neurosci* 33:14211–14224.
32. Adhikari A, Topiwala MA, Gordon JA (2010) Synchronized activity between the ventral hippocampus and the medial prefrontal cortex during anxiety. *Neuron* 65:257–269.
33. Fujisawa S, Buzsáki G (2011) A 4 Hz oscillation adaptively synchronizes prefrontal, VTA, and hippocampal activities. *Neuron* 72:153–165.
34. Karalis N, et al. (2016) 4-Hz oscillations synchronize prefrontal-amygdala circuits during fear behavior. *Nat Neurosci* 19:605–612.
35. Dejean C, et al. (2016) Prefrontal neuronal assemblies temporally control fear behaviour. *Nature* 535:420–424.
36. European Science Foundation (2001) Use of animals in research, European Science Foundation Policy Briefing, 2nd Ed. Available at archives.esf.org/fileadmin/Public_documents/Publications/ESPB15.pdf. Accessed March 28, 2017.
37. National Research Council (2011) *Guide for the Care and Use of Laboratory Animals* (National Academies Press, Washington, DC).
38. Paxinos G, Franklin KBJ (2001) *The Mouse Brain in Stereotaxic Coordinates* (Academic, San Diego).
39. Brankačk J, Kukushka VI, Vyssotski AL, Draguhn A (2010) EEG gamma frequency and sleep-wake scoring in mice: Comparing two types of supervised classifiers. *Brain Res* 1322:59–71.